

Investigation and Mitigation of Sputter Damage on Co-Evaporated Cu(In,Ga)Se₂ Absorbers for Photovoltaic Applications

Ramis Hertwig,* Shiro Nishiwaki, Ayodhya N. Tiwari, and Romain Carron

Herein, the detrimental impact of radio frequency (RF)-sputtering on bare Cu(In,Ga)Se₂ photovoltaic absorbers in view of vacuum-deposited buffer layers is evaluated, and the possible mitigation strategies are explored. Carrier lifetimes are measured using time-resolved photoluminescence before and after buffer deposition and exposure to the plasma environment. When directly applied on bare Cu(In,Ga)Se₂ absorbers, RF-sputtering is severely limiting the device performance, with oxygen ions emanating from the target having a stronger effect than argon ions from the process gas. The possibilities to avoid sputter damage by atomic layer deposited Zn_{1-x}Mg_xO and chemical bath deposited CdS buffer layers are shown, and the ability of the latter to restore damaged surfaces is highlighted. Absorber performance is also investigated for absorbers stored in air, N₂, or ultra-high vacuum. The reduction in carrier lifetime is reflected in the reduced open-circuit voltage of solar cells. SCAPS simulations are used to investigate possibilities to minimize the effect of sputter damage. Finally, options on how to minimize sputter damage during buffer deposition as well as on how to modify the absorber to be less sensitive are discussed.

breaks the chain of vacuum-based device processing of adjacent absorber and transparent conducting oxide (TCO) layers. Although large efforts have been undertaken to find suitable alternatives for CBD-CdS, the power conversion efficiency (PCE) of Cd-free devices has only recently surpassed the PCE of Cd-buffered photovoltaic cells based on Cu(In,Ga)(S,Se)₂.^[1,3] The alternative to CdS should be a material with a larger bandgap, compatible with the absorber in terms of band alignment and lattice constant, and suitable for the subsequent deposition of TCO as high- and low resistance windows (HRW, LRW).

High optoelectronic quality TCO is mostly deposited using magnetron sputtering, as this method is scalable, reproducible, and controllable. Magnetron sputtering is a vacuum-based deposition technique, which utilizes a plasma, that


1. Introduction

Chalcopyrite semiconductors such as Cu(In,Ga)Se₂ (CIGS) are promising absorber materials for thin-film solar cells for delivering high power conversion efficiency, performance stability, and possibility for low-cost manufacturing.^[1,2] One possibility to improve device performance and reduce the complexity of the fabrication process is to substitute the chemical bath deposited (CBD)-CdS buffer layer with an alternate layer and deposition process. CdS is classified as toxic, and contributes to parasitic optical absorption due to the low bandgap of 2.4 eV and therefore reduced current, while the CBD process

is ignited via direct current (DC) or radio frequency (RF). The plasma-generated gas ions bombard and thereby liberate particles from the target, which are then transferred to the substrate. The exposure of the substrate to plasma emission, particles, and heat can harm sensitive substrates by generating defects or structural changes, thereby compromising device performance. Sputter damage is frequently suggested as an explanation for less than ideal device behavior,^[4-7] albeit direct investigations of sputter damage on CIGS are rare.^[8,9] Sputter damage in perovskite or Si solar cells has been reported.^[10,11]

Solar cells based on CIGS show very poor behavior when the TCO is directly sputtered on top of the absorber. The addition of S in the absorber or buffer layer seems to improve the cell behavior,^[3,12,13] which can be explained by a lower valance band at the interface and the accompanied repulsion of holes. Historically, the buffer layer was deposited using a soft deposition method, where CBD-CdS resulted in the best performing devices.^[14] The protection of the absorber from plasma damage is a crucial factor to achieve high V_{OC} and FF, and will be investigated in this work. We chose atomic layer deposited (ALD) ZnMgO as buffer material, due to its higher bandgap (>3.2 eV) and shifting conduction band position depending on the Mg content, as well as uniform coverage. Cu(In,Ga)Se₂ absorbers with and without buffer layers have been exposed to Ar plasma under HRW deposition conditions and the charge

R. Hertwig, S. Nishiwaki, A. N. Tiwari, R. Carron
Laboratory for Thin Films and Photovoltaics
Empa - Swiss Federal Laboratories for Materials Science and Technology
8600 Duebendorf, Switzerland
E-mail: ramis.hertwig@empa.ch

 The ORCID identification number(s) for the author(s) of this article can be found under <https://doi.org/10.1002/solr.202200268>.

© 2022 The Authors. Solar RRL published by Wiley-VCH GmbH. This is an open access article under the terms of the Creative Commons Attribution-NonCommercial License, which permits use, distribution and reproduction in any medium, provided the original work is properly cited and is not used for commercial purposes.

DOI: 10.1002/solr.202200268

carrier lifetime has been investigated. The correlation between sputtering conditions, absorber surface, carrier lifetime, and device performance are discussed and supported with 1D SCAPS simulations.

2. Experimental Section

CIGS absorbers were grown on soda-lime glass (SLG) with a sputtered Mo rear contact using the three-stage process described in ref. [15]. The reference device has a buffer layer of CBD-CdS, the HRW consisting of RF-co-sputtered iZnO/MgO, and the LRW of ZnO:Al. The target diameters are 100 mm for iZnO and MgO and 250 mm for ZnO:Al. For co-sputtered Zn_{0.9}Mg_{0.1}O the MgO power is 1.4 times the power of the ZnO target. Electronic contacts are applied via e-beam evaporated Ni-Al grids. The cell area is defined by mechanical scribing and determined using a flatbed scanner. Buffer layers consisting of ZnO, MgO, and Al₂O₃ were deposited by atomic-layer deposition (ALD) in a Fiji G2 system (Ultratech). Ar was used as a carrier gas with a base pressure of 0.13 mbar. The respective precursors are diethylzinc (DEZ), bis(cyclopentadienyl)magnesium (MgCp2), trimethylaluminum (TMA), and H₂O. MgCp2 was preheated to 90 °C, and the substrate as well as the reaction chamber and all delivery lines were kept at 150 °C. CdS buffer layers were grown in a stirred solution consisting of 185 mL, H₂O, 35 mL NH₄OH, 15 mL Cd-acetate, and 15 mL thio-urea (TU) for 14 min at 70 °C.

I–V characterization was carried out with a Keithley 2400 source meter and four-terminal contacting under standard test conditions (1000 W m^{−2}, 298 K) using an ABA-type solar simulator on relaxed samples unless stated otherwise. TRPL measurements were performed using a 639 nm diode laser with 100 ps pulse duration as excitation source, and an InGaAs photomultiplier in combination with a PicoQuant time-correlated single photon counting electronics for signal acquisition. Pulse repetition rates varied between 0.1 MHz and 3 MHz. The illumination spot size was around 130 μm in diameter. The corresponding photon density was around 3 × 10¹¹ cm^{−2} per pulse. The time between surface treatment or buffer deposition until TRPL measurement was kept below 10 min. Measurements have been taken with either 0.05 ns or 2.5 ns per channel. A variation of ≈ factor 2 in the peak intensity can be caused by a minimal drift of the optical components in the measurement system. For samples with ALD buffer, the deposition time at 100 °C could affect the absorber doping, which can explain variations in intensity. Therefore, the analysis of the difficult to extract factor A is omitted. The data is corrected for background and normalized, then fit with a double exponential function according to Equation (1). The effective carrier lifetime τ_{eff} is calculated from the weighted average given in Equation (2).

$$Y = A_1 \cdot \exp\left(-\frac{t}{\tau_1}\right) + A_2 \cdot \exp\left(-\frac{t}{\tau_2}\right) \quad (1)$$

$$\tau_{\text{eff}} = \frac{(A_1 \cdot \tau_1) + (A_2 \cdot \tau_2)}{A_1 + A_2} \quad (2)$$

The decrease in lifetimes before and after introducing sputter damage can be associated with a difference in V_{OC} . By following

the detailed balance principle, the V_{OC} can be correlated to the ratio of τ_{eff} as shown in Equation (3).^[16] Here, k is the Boltzman constant, q the electron charge, and T the temperature in Kelvin.

$$\Delta V_{\text{OC}} = \frac{kT}{q} \ln\left(\frac{\tau_{\text{sample}}^{\text{eff}}}{\tau_{\text{ref}}^{\text{eff}}}\right) \quad (3)$$

SCAPS version 3.3.05^[17] was used to model a layer stack of CIGS/CdS/ZnO/AZO to analyze variations at the front interface. Therefore, no Mo rear contact and no CIGS absorber grading are implemented. Detailed parameters are given in Table 1. The implementation of defects is described in Section 4.5. The CdS layer is implemented with a minimal layer thickness of 0.1 nm to circumvent simulation convergence issues.

3. Results and Discussion

The following sections examine the effects of sputtering, aging in different environments, and buffer deposition on the effective charge carrier lifetime in CIGS absorbers to estimate the maximal possible V_{OC} and therefore device performance.

3.1. Influence of Sputter Parameters on Carrier Lifetime

To demonstrate the sensitivity of the CIGS absorber surface and the concomitant necessity for an appropriate protective layer, Zn_{1−x}Mg_xO has been co-sputtered from ZnO and MgO targets on CIGS absorbers for 10 s. The targeted stoichiometry is $x = 0.1$, with applied power at the MgO target 1.4 times the power of the ZnO target. Hereafter, only the ZnO power is stated, since ZnO is the parent material and MgO power can be determined accordingly. Immediately before entering the deposition chamber, CIGS absorbers have been rinsed in NH₄OH for 1 min,^[18] to remove alkali crystals and prepare the surface in a reproducible manner. The time between rinsing the absorber and introducing it to the deposition chamber is less than 10 min. In the deposition chamber, the ZnO and MgO target have been pre-sputtered without the presence of the target for three minutes, so that a clean target surface is present. ZnMgO has been deposited at varying powers from 25 to 100 W (0.079 to 0.318 W cm^{−2}). The growth rates for co-sputtered Zn_{0.9}Mg_{0.1}O

Table 1. Layer parameters for SCAPS simulation.

	CIGS	CdS	i ZnO	AZO
Thickness [nm]	2000	0.1	70	200
Bandgap, ungraded [eV]	1.2	2.48	3.37	3.37
Electron affinity [eV]	4.5	4.4	4.5	4.5
Dielectric permittivity (relative)	13.6	10	10	8.49
CB effective density of states [1 cm ^{−3}]		2.20E + 18		
VB effective density of states [1 cm ^{−3}]		1.80E + 19		
Electron thermal velocity [cm s ^{−1}]		2.63E + 07		
Hole thermal velocity [cm s ^{−1}]	1.30E + 07		2.63E + 07	
Electron mobility [cm ² V ^{−1} s ^{−1}]		5.00E + 01		
Hole mobility [cm ² V ^{−1} s ^{−1}]		5.00E + 01		

are 2.5 nm min^{-1} for 25 W and 12.8 nm min^{-1} for 100 W, determined by ellipsometry of $\text{Zn}_{1-x}\text{Mg}_x\text{O}$ layers deposited on Si. The power was ramped up from 50 W to the desired power within 60 s, after which the target shutter was opened for 10 s. After closing the shutter, the plasma is turned off within 30 s. The carrier lifetimes are determined by TRPL measurements within 10 min after extraction from the vacuum chamber. Lifetimes before and after sputtering are displayed in Figure 1a.

TRPL measurements reveal a significant decrease in the carrier lifetime with an increase in sputtering power, see Figure 1a. The lifetimes decrease from 333 ns without sputter deposition to $\approx 5 \text{ ns}$ after 100 W for 10 s. Decreasing the background pressure from 1×10^{-3} to 1×10^{-2} mbar decreases the associated lifetimes from 34 to 17 ns, while doubling the deposition time to 20 s decreases the carrier lifetime to 13 ns, both at 50 W. It is fair to assume that the deposited layer itself has a minor influence on the carrier lifetime since the maximal layer thickness is $\approx 2 \text{ nm}$. Also, the film thickness of sputtered $\text{Zn}_{1-x}\text{Mg}_x\text{O}$ for 50 W and 20 s is the same as 100 W and 10 s, but lower powers have a milder effect on the carrier lifetime. These results suggest that even with a very low deposition power, which would lead to slow growth rates, the loss in carrier lifetime, and therefore V_{OC} is not acceptable for high performing photovoltaic devices. Such a process would not be suitable for industrial production, where the growth rate could be larger than 10 nm s^{-1} .

These results raise the question of what the sputter deposition actually does to the absorber surface that reduces the V_{OC} so drastically. The $\text{Zn}_{1-x}\text{Mg}_x\text{O}$ material itself is unlikely to be the cause of recombination centers, because devices with a CdS buffer layer and RF sputtered $\text{Zn}_{1-x}\text{Mg}_x\text{O}$ as HRW 70 nm show no strong decrease in V_{OC} , which will be elaborated later (Figure 4b), and ALD deposited $\text{Zn}_{1-x}\text{Mg}_x\text{O}$ even shows an increase in carrier lifetime, see Section 4.2. Therefore, we analyze the species present during sputter deposition and the involved quantities and energies. The sputtering process in this work involves pure Ar plasma, which exposes the sample to Ar ions, electrons, and radiation. Additionally, ions from the target and a magnetic field from the magnetron are present. Since there is no report of the influence of magnetic fields on the surface composition of CIGS, this effect is neglected. The effect of the plasma radiation is discussed next.

Ar radiation in a DC or RF plasma appears purple to the human eye, which is an aggregation of radiative wavelengths in the range of $\approx 200\text{--}900 \text{ nm}$ or 6.2 eV to 1.38 eV , respectively.^[19,20] Notable peaks of intensity are at 280, 310 nm, the peaks with the highest intensity are between 400, 450, and 600 nm. Those wavelengths are absorbed by the CIGS surface, where the bandgap is around 1.2 eV , and not attenuated by the growing ZnMgO thin film with a bandgap of more than 3.2 eV . Absorbers with $\text{Zn}_{1-x}\text{Mg}_x\text{O}$, where one half has been taped with Kapton on top (polyimide, $E_g \approx 2.9 \text{ eV}$) show almost no decrease in carrier lifetime. Wavelengths in the UV are not known to harm CIGS, but rather induce metastable effects depending on the absorber/buffer interface.^[21–24] Additionally, the intensity of plasma radiation does barely scale with applied power, but rather with pressure. Together, this leads to the conclusion that the damage is not radiation based.

Next, the direct interaction of ions with the CIGS surface is discussed. Two mechanisms are possible: ion implantation and agglomeration of charges. Before analyzing the influence of either, the possible ions and their occurrence is stated. Ar^+ and O^- are known to be the most abundant species present during ZnO or MgO deposition from ceramic targets in an Ar atmosphere.^[25–27] Ar^+ are 100 times more prevalent than Zn^+ , whereas O^- are 100 times more prevalent than O^{2-} . Other species were even less common. It is worth mentioning, that while the Ar^+ ions can only originate from the Ar gas, oxygen ions can also originate if oxygen gas is mixed into the Ar. In the experiments conducted in the studies mentioned earlier, the oxygen originates almost exclusively from the target, even when an argon oxygen mixture was used. Depositions from a MgO target did show virtually the same distribution of ions as for ZnO. For further analysis, it is assumed that if the absorber surface is altered by positive or negative ions, it is related to Ar^+ or O^- .

The ionic radius of Ar is difficult to measure, since it rarely forms bonds with other elements. For the sake of discussion, the van der Waals radius of 1.88 \AA is used. The lattice constant of the smallest species possibly present on the CIGS surface is CuSe with 3.79 \AA (CuS 3.79 \AA , compared to CuInSe₂ with 5.78 \AA and CuGaSe₂ with 5.61 \AA (CuInS₂ 5.52 \AA , CuGaS₂ 5.35 \AA).^[28] The interatomic distance of neighboring atoms is in the range of $2\text{--}2.5 \text{ \AA}$,^[29] which means that Ar^+ could spatially fit into

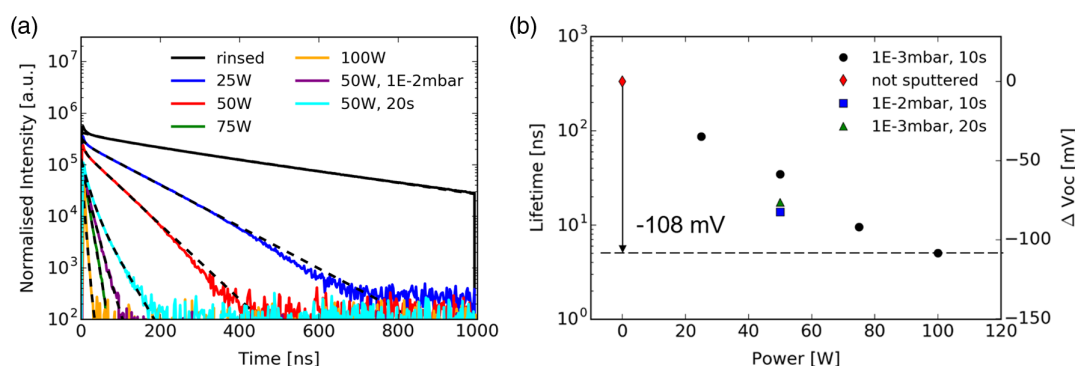


Figure 1. a) Decrease of carrier lifetime with increased sputter power of ZnMgO on rinsed Cu(In,Ga)Se₂ (CIGS) absorbers as measured with time-resolved photoluminescence (TRPL). The effect of longer exposure (20sec) and higher background pressure (1×10^{-2} mbar) are shown as well. b) Comparison of TRPL lifetimes correlated with the calculated difference in V_{OC} of solar cells with unsputtered absorber and after 10 s at 100 W.

the CIGS absorber surface. The same is true for O^- with a van der Waals radius of 1.52 Å. Furthermore, the energy of O^- ions is reported to span a range up to 400 eV, with an average of around 200 eV, while Ar^+ shows energies of 20–40 eV. The binding energies of Cu, In, Ga, and Se to each other are reported to be just in the few eV,^[30,31] so it seems perfectly feasible for O^- to break those bonds upon impact. The ion implantation, be it Ar^+ or O^- , would lead to increased lattice defects around the site of implantation. At this point, ion implantation is not implausible. For direct evidence of ion implantation and the related defects, GI-XRD needs to be performed, which we did not do.

Other than being implanted and generating defects or dangling bonds, ions could stick to the surface and accumulate charges, which can lead to Fermi level pinning (FLP). While the Fermi-level position is usually defined by doping, it can be fixed to a position of peak surface state density. This can be in the form of accumulated charges in terms of defects, or surface termination. Both are common at interfaces. Fermi-level pinning is a frequent phenomenon in GaAs solar cells^[32] and has also been observed in CIGS, where commonly reported values for V_{OC} coincide with the most common defect position in the respective material.^[33–35] FLP can explain low V_{OC} and FF in completed devices, but the effect observed here is a continuum of degradation. Hence, it does not seem to relate to specific defect energies, but rather to a distribution of recombination centers. FLP could still be a mechanism that limits CIGS solar devices, but the literature on that topic is indecisive.^[36–39]

3.2. Aging and Recovery of CIGS Absorbers

The results from the previous experiment strongly suggest that the decrease in carrier lifetime originates in an altered surface state, either chemically by altering the absorber surface, or by pinning the Fermi level via dominant surface charges. After considering the degradation of the CIGS surface during sputtering, we now investigate the effect of storage on the absorber surface and possible performance losses related to it. A set of rinsed

absorbers was kept in ambient air, N_2 , and ultra-high vacuum (1×10^{-6} mbar) for 7 and 21 days, respectively. Carrier lifetime has been characterized before and after storage. Additionally, CBD–CdS and ALD ZnMgO have been applied as buffer layers to evaluate the respective impact on the carrier lifetime. The results are summarized in Figure 2.

For all three storage environments, the carrier lifetime decreases. The decrease is fastest in air and slowest in UHV. Absorbers stored in the air have a large decrease in their carrier lifetime from 352 ns to 13 ns within 7 days, while the same absorber deposited with ALD ZnMgO (28 nm) decreases from initially 468 to 84 ns, see Figure 2a. The deposition of the ALD ZnMgO film before storage increased τ_{eff} and significantly slowed the degradation. The carrier lifetime of rinsed absorbers stored in UHV or N_2 decreases from initial 354–156 and 30 ns, respectively. Lifetime recovers to 229 and 78 ns upon deposition of 30 nm of CBD–CdS after the aging experiment. In all cases, a decrease in τ_{eff} over time and an increase after buffer deposition can be found. It stands to reason that these two effects originate from the same mechanism, and are working opposites.

The aging of absorbers could be related to oxygen, which would explain the accelerated degradation once O_2 is added to the sputtering gas.^[8] Since oxygen is present in large quantities in air, it is also adsorbed on the absorber surface. When stored in air, steady partial pressure of oxygen is present at the CIGS surface. In the N_2 atmosphere under the same pressure, only the oxygen adsorbed at the surface is present, which limits the degradation over time. On the other hand, samples stored in UHV have no oxygen and low pressure, which could lead some of the oxygen to desorb, leaving the surface with a smaller initial oxygen supply, and therefore degrading even slower. The opposite recovery effect after buffer deposition could therefore simply be a removal of oxygen and oxygen compounds from the absorber surface, which is known to happen in CBD due to the addition of NH_4OH .^[40,41] Due to its dielectric nature, the ALD-deposited Al_2O_3 could passivate surface defects related to oxygen instead of removing the material, resulting in regeneration of the absorber via reducing recombination velocities at the interface.^[42] This

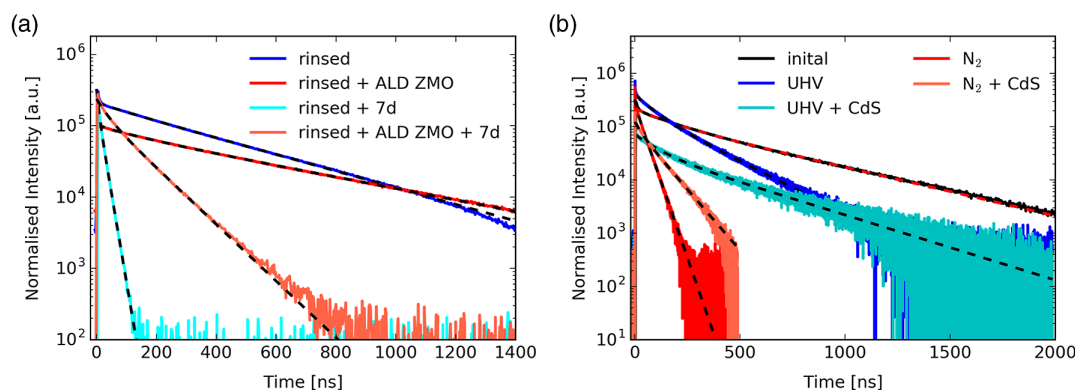


Figure 2. a) TRPL measurement for fresh CIGS absorber with and without atomic layer deposited (ALD) $Zn_{1-x}Mg_xO$ compared to the same absorber after storage in air for seven days. In both cases, the lifetime decreases strongly with time. The initial and aged lifetime of the absorber covered in ALD $Zn_{1-x}Mg_xO$ is higher than without $Zn_{1-x}Mg_xO$. b) TRPL measurements of CIGS absorbers before and after 21 days storage in N_2 or UHV. The carrier lifetime for both absorbers decreases, although the decrease after storage in UHV is significantly less than after storage in N_2 . The carrier lifetime increases after the application of chemical bath deposited (CBD)–CdS in both cases, although not to the initial level.

effect should be taken into account when encapsulating CIGS absorbers in a layer similar to a buffer layer for storage as done in ref., [43] since the encapsulation and etching might induce regeneration. At this point, it is not clear whether regeneration is the opposite effect of aging or a result of the formation of a pn-junction.^[44]

The measured τ_{eff} cannot be separated clearly in bulk and surface lifetimes τ_b and τ_s with the experiments done here. Specific considerations have to be made to disentangle the respective lifetimes according to Equation (4), but even then the possible parameter space can only be reduced.^[45] Nevertheless, upper and lower limits for τ_s and τ_b could be extracted from the measured TRPL data, when the assumptions are made accordingly. First, one can neglect bulk recombination, then τ_{eff} equals τ_s . We would directly measure the surface lifetime, so all reported lifetimes equal the surface lifetime. Second, a value for the bulk lifetime τ_b can be estimated by assuming τ_s is infinite before treatment/aging. Then, the reported lifetimes before the introduction of sputter damage would equal the bulk lifetime, and considering τ_b to be unchanged after sputtering, the reduced surface lifetime can be calculated. This approach does not model the data appropriately since the addition of ALD ZnMgO increases the surface lifetime, which was initially set to be infinite.

$$\frac{1}{\tau_{\text{eff}}} = \frac{1}{\tau_b} + \frac{1}{\tau_s} \quad (4)$$

3.3. Effect of Ar Ions

The effects of Ar^+ and O^- should be looked into separately. Therefore, CIGS absorbers buffered with either CBD-CdS (30 nm) or ALD Al_2O_3 and $\text{Zn}_{1-x}\text{Mg}_x\text{O}$ (28 nm) are first exposed to pure Ar^+ plasma, which is ignited on the top of the sample without the involvement of an oxide target, at 100 W for 5 min each. This way, only the interaction with Ar^+ is reflected in the changes in the measured carrier lifetime, see Figure 3a. The carrier lifetimes in absorbers with ALD Al_2O_3 and $\text{Zn}_{1-x}\text{Mg}_x\text{O}$ buffer change from 214 ns before plasma exposure to 242 ns after plasma exposure, while in CBD-CdS buffered absorbers it changes from 224 to 162 ns. The slight increase

for the ALD-buffered devices corresponds to a few mV differences in V_{OC} according to Equation (3), and is within the distribution range of lifetimes that are measured on the same sample (± 15 ns are common). This is also true for the change in lifetime for CBD-CdS-buffered devices, where the difference in lifetime results in a ΔV_{OC} that is within the distribution range of V_{OC} of cells for the same absorber (usually ± 10 mV). We, therefore, conclude that the influence of Ar^+ on the buffered absorber is negligible. The lifetimes of samples exposed to plasma from an Ar/O_2 gas mixture could not be measured, but the effect has been investigated in ref. [8]

3.4. Solar Cells with and Without Buffer Layer

The effect of direct RF sputtering of the HRW window on the device performance is examined by completing CIGS cells with different structures of the window layer. For clarity, the term buffer layer is used in regards to CBD-CdS and ALD $\text{Zn}_{1-x}\text{Mg}_x\text{O}$, while window layer refers to sputtered TCO. Rinsed CIGS absorbers without buffer layer were RF sputtered directly with $\text{Zn}_{1-x}\text{Mg}_x\text{O}$ ($x=0.1$) with 22, 67, and 112 W. Absorbers with CBD CdS buffer layer were sputtered with 50 W. CIGS absorbers with ALD $\text{Zn}_{1-x}\text{Mg}_x\text{O}$ ($x=0.16$) buffer layer had the window layer applied with 80 W. Dark and illuminated JV curves are displayed in Figure 4a,b. First, the devices without a buffer layer are analyzed (dashed lines). Devices without a buffer layer exhibit a high diode factor of more than 2.4 for 112 and 2.2 for 22 W, paired with a fairly low parallel resistance (R_p) of less than $2000 \Omega\text{cm}^2$. Devices with buffer layer show diode factors of 2.1 for the ALD $\text{Zn}_{1-x}\text{Mg}_x\text{O}$ buffer and 1.6 for the CBD-CdS buffer, with R_p of 1317 and $8375 \Omega\text{cm}^2$, respectively. In the illuminated JV, the most prominent feature is the decrease of V_{OC} with increasing sputter power for the buffer free devices of roughly 1 mV W^{-1} . Furthermore, the devices show a violation of shifting approximation upon illumination. This hints at additional problems with the buffer-free devices regarding charge extraction or blocking of the photocurrent. Further analysis of the JV curves with sputtered buffer layer, e.g., a double diode model would necessitate diode factors A of less than 2, otherwise, the association of different recombination pathways

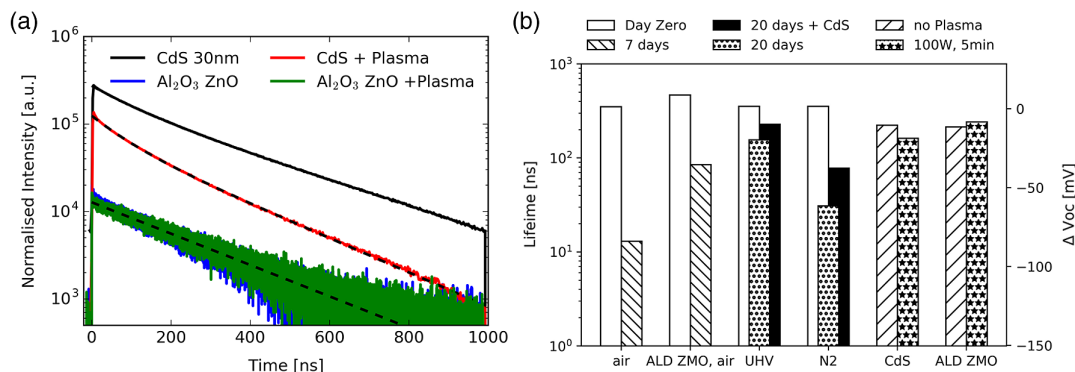


Figure 3. a) TRPL measurement of CIGS absorbers covered with CBD-CdS compared to absorbers covered in ALD Al_2O_3 and $\text{Zn}_{1-x}\text{Mg}_x\text{O}$ before and after exposure to Ar plasma. The decrease of carrier lifetime for absorbers with CdS is visible, but the resulting loss in V_{OC} is small. The lifetime of absorbers covered with ALD Al_2O_3 and $\text{Zn}_{1-x}\text{Mg}_x\text{O}$ is unchanged. b) Summary of investigation of carrier lifetimes for absorbers stored in air, UHV, N_2 as well as absorbers covered in CBD-CdS or ALD Al_2O_3 and $\text{Zn}_{1-x}\text{Mg}_x\text{O}$ before and after exposure to Ar plasma.

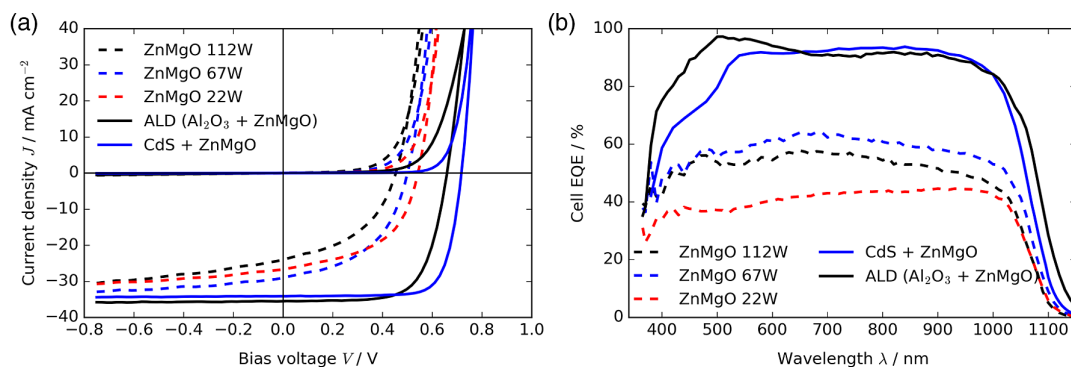


Figure 4. a) Dark and illuminated JV for CIGS solar cells without (dashed) and with (solid) buffer layer and sputtered window layers. b) External quantum efficiency (EQE) of same samples. The EQE is decreased flat, which further indicates problems of charge extraction at the interface.

Table 2. PV parameters of devices with RF sputtered or ALD $\text{Zn}_{1-x}\text{Mg}_x\text{O}$ buffer layers. The CBD–CdS buffer layer device is given for reference.

Sample	J_{sc} [mA cm^{-2}]	V_{oc} [V]	FF [%]	PCE [%]	A (dark)	R_p [$\Omega \text{ cm}^2$]
ZnMgO 112 W	23.93	0.453	45.3	4.9	2.42	999
ZnMgO 67 W	28.96	0.500	45.6	7.0	2.41	1911
ZnMgO 22 W	26.61	0.543	51.3	7.4	2.25	1689
ALD ($\text{Al}_2\text{O}_3 + \text{ZnMgO}$)	35.51	0.659	68.7	16.1	2.1	1318
CdS + ZnMgO	34.10	0.718	76.3	18.6	1.6	8375

is not clearly identifiable. Devices with a buffer layer, on contrast, show higher V_{oc} , J_{sc} , and FF, regardless of the deposition method or material. The diode behavior is significantly better in both dark and illumination conditions. Detailed PV parameters can be found in Table 2. The difference between direct RF sputtering onto the absorber and sputtering onto a buffer layer is obvious. The presence of a buffer layer before sputter deposition improves significantly all metrics performance. This leads to the conclusion that both buffer layers tested here (CBD–CdS and ALD $\text{Zn}_{1-x}\text{Mg}_x\text{O}$) shield the absorber surface sufficiently from the previously discussed effects.

3.5. Defect Simulation

The large difference in V_{oc} for devices with and without buffer layer shows the importance of controlling recombination at the absorber surface. To analyze the influence of the defect density (DD), defect energy (DE), and capture cross-section (CSS), a SCAPS model with the parameters shown in Table 1 has been simulated. Additionally, to the layer properties, the model uses AM 1.5 light spectrum for illumination, as well as no series resistance and infinite parallel resistance. The values have been chosen to match the JV of the reference device with the CdS buffer layer depicted in Figure 4b. Since higher sputtering powers are assumed to introduce more of the same defects in the absorber surface, the sputter power is represented by the total defect density in the interface between absorber and buffer.

DD has been varied from 1×10^8 to $1 \times 10^{16} \text{ cm}^{-2}$, DE from 0.2 to 1.0 eV with respect to the valance band position of the 1.2 eV bandgap of the absorber, CCS has been varied from 1×10^{-10} to $1 \times 10^{-20} \text{ cm}^2$. The simulations show a strong dependence of the JV behavior on the DD, with low DD resulting in better devices. The influence of DE is significantly smaller, and shows only when close to the conduction band, as plotted in Figure 5. The CCS has virtually no impact on the JV behavior for the scanned range, hence it is not presented here.

Since the difference between those devices is the presence or absence of a buffer layer, it is fair to assume that the interface between the absorber and the neighboring layer is the decisive factor for the cell behavior, especially since the detrimental effect of the $\text{Zn}_{1-x}\text{Mg}_x\text{O}$ layer has been ruled out earlier (Section 4.2). We test the hypothesis of defects being generated at the absorber surface when exposed to plasma ions by simulating a CIGS solar cell with different DD at the absorber/buffer interface in SCAPS, see Figure 4a. The DD has been varied from 1×10^8 to $1 \times 10^{16} \text{ cm}^{-2}$, while the DE (midgap, 0.6 eV), and CCS $1 \times 10^{-15} \text{ cm}^2$ have been kept constant. As expected, the V_{oc} decreases with increasing DD, which can in return be attributed to higher plasma power. Further investigations on the DE and CCS reveal that the influence of those parameters is significantly smaller than that of the DD. A scan of different DE is depicted in Figure 5a, where minimal variations are visible. For other CCSs, the influence on the JV curve is even less (not shown here.) The reverse effect, the improvement of cell behavior as a result of fewer defects, has been shown in ref. [46]

Since the presence of positive and negative ions during sputter deposition is difficult to mitigate, sputter damage will always be present to some degree. The following analysis from the point of view of the band alignment at the absorber/buffer interface suggests an additional way to minimize performance loss, by including S in the absorber surface to lower the valence band. The top 20 nm of the $\text{Cu}(\text{In,Ga})\text{Se}_2$ absorber is replaced with a $\text{Cu}(\text{In,Ga})(\text{S,Se})_2$ layer which allows to vary the bandgap to simulate the introduction of S into the absorber surface. Then, the influence of the layer thickness, bandgap in relation to the DD at the interface on device performance is analyzed. A schematic representation of the band alignment and the simulated results are given in Figure 6.

The penetration depth of S, which is modeled by the absorber top layer with a higher bandgap, shows only a minimal effect on

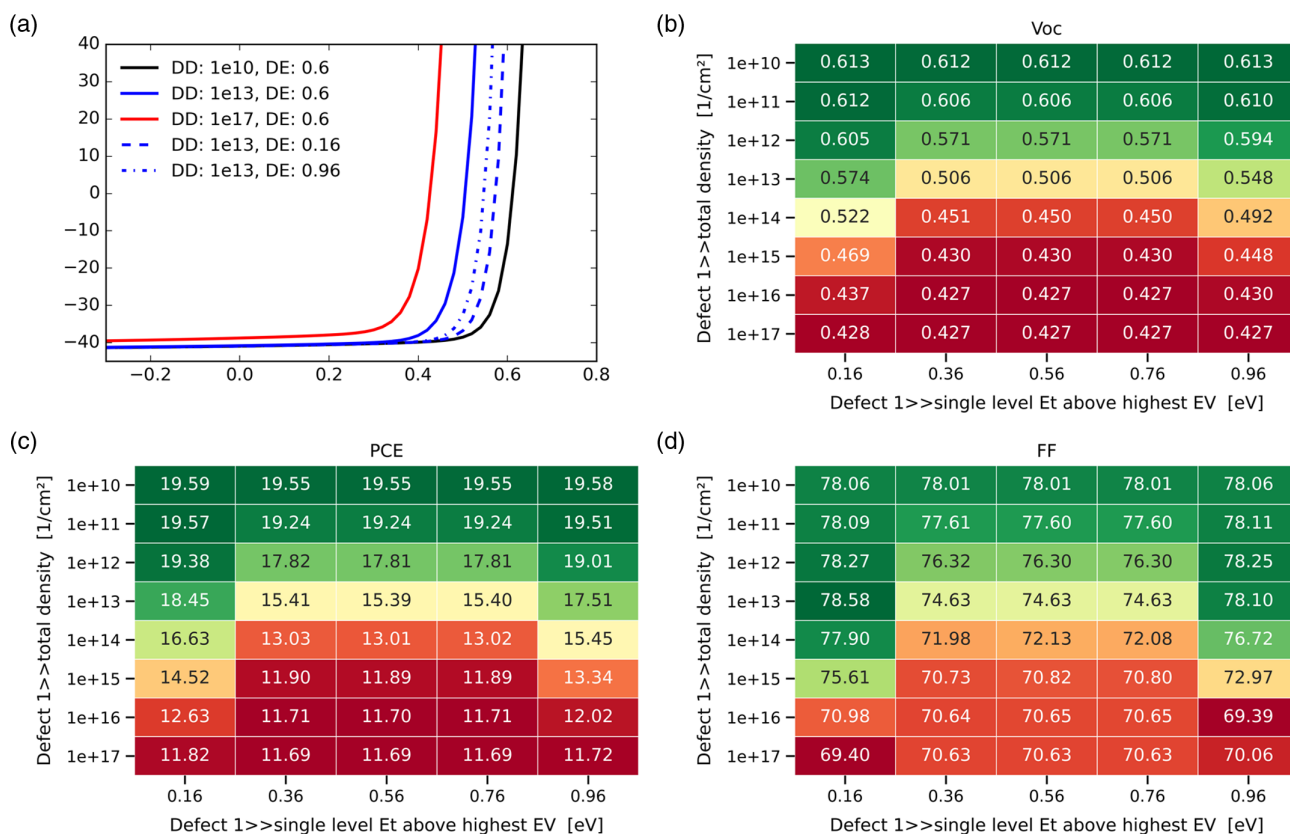


Figure 5. SCAPS simulation of device with increasing DD at different DE levels at the absorber/buffer interface. a) J/V of selected parameter combinations. b–d) Heatmap of parameter combinations for V_{oc} , power conversion efficiency (PCE), and fill factor (FF). J_{sc} is not shown since the variations are minimal.

the device performance (not shown). The heatmaps display the influence of the absorber surface bandgap on the y-axis and the DD on the x-axis with the device V_{oc} and efficiency. The influence on the J_{sc} is minimal, hence it is not shown here. The FF is displayed in Figure 5d. The V_{oc} varies from a minimal 0.406 to 0.613 V, and the efficiency from 10.77% to 19.55%. The variation in device efficiency is a direct result of the variations in the V_{oc} , hence the evolution with the absorber surface bandgap and DD is equivalent. As before, the V_{oc} decreases with more defects at the interface, but here the effect is less pronounced for larger surface bandgap energies. The difference in V_{oc} for a given DD can be more than 100 meV higher when the valence band maximum is decreased by 0.1 eV, which is attributed to a better repulsion of holes away from the absorber buffer interface. Absorber surface sulfurization can be used to make the CIGSe absorber more resilient to sputter damage, as has presumably been demonstrated by,^[3] under specific sputter conditions (off center, low power).

4. Summary and Conclusion

In summary, we have investigated the effect of sputter damage on CIGSe absorber with TRPL and shown the detrimental effects

of sputter damage in full solar cells. The progressive decrease in τ_{eff} with sputtering power indicates a dominant interaction with O^- , followed by Ar^+ . Further degradation mechanisms could be observed when bare absorbers were stored in air, N_2 , and UHV. Higher sputter powers during the deposition of buffer layers lead to worse device performance, hence low sputtering powers or other deposition methods need to be considered as compared to sputtered ZnMgO. The protective and regenerative qualities of ALD- $Zn_{1-x}Mg_xO$ and CBD- CdS have been demonstrated, with an increase in carrier lifetime after buffer deposition and more than 100 meV in the device V_{oc} for non-optimized cells, as well as improved diode behavior. Numerical SCAPS simulations have been carried out, where the severity of sputter damage has been modeled with defects at the absorber surface. The simulations show that the DD has a far greater influence on device performance than the DE position or the CSS. Furthermore, simulations show that the detrimental effect can be reduced by lowering the valence band near the absorber surface, which acts as a barrier for holes, therefore reducing recombination at the interface. We believe that the effective mitigation of sputter damage, as well as the incorporation of S in the absorber, are two major reasons for the high device efficiencies demonstrated with Cd-free buffer layers in ref. [1,3]

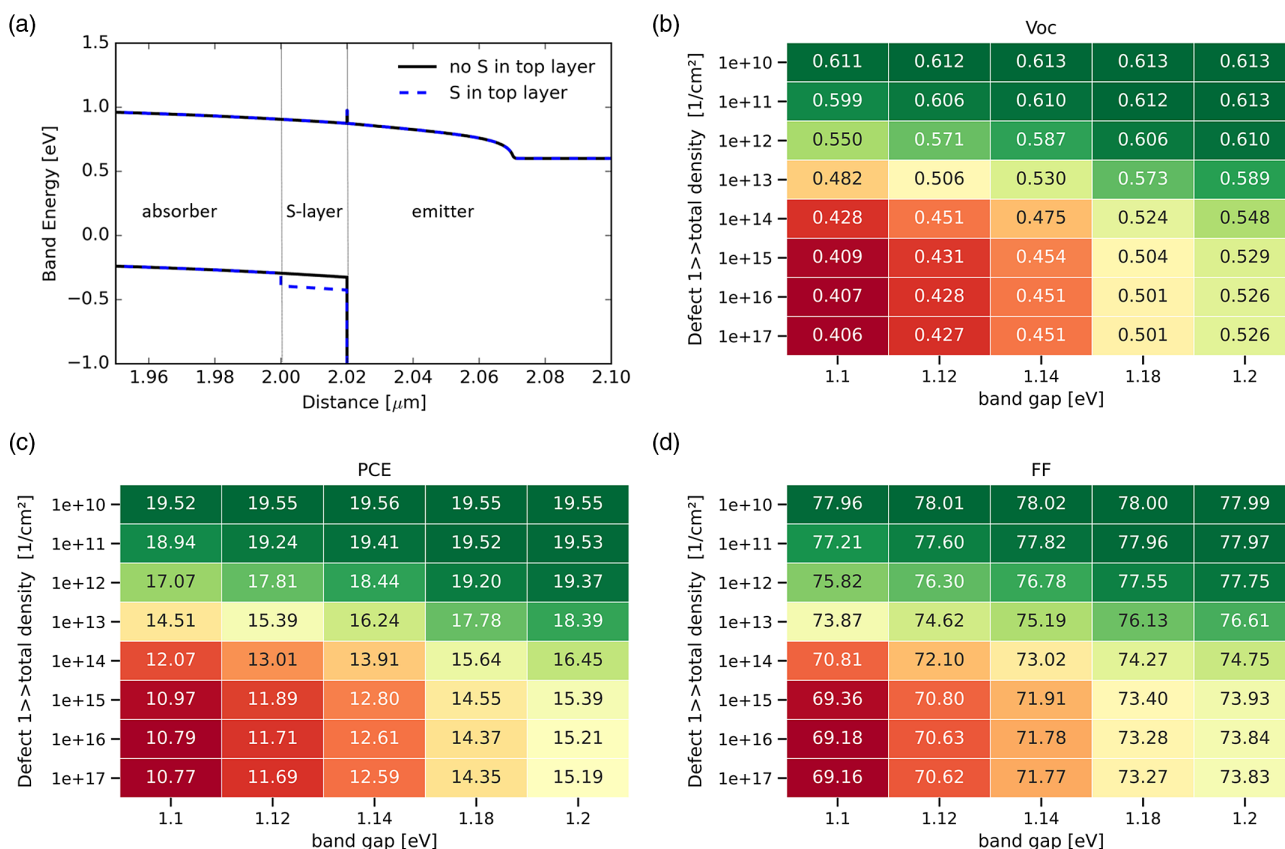


Figure 6. SCAPS simulation of CIGSSe device with higher absorber surface bandgap to represent S incorporation. a) Comparison of band structure with and without S at the absorber buffer interface. b–d) Heatmap of parameter combinations for Voc, PCE, and FF. Jsc is not shown since the variations are minimal.

Acknowledgements

This project has received funding from the European Union's Horizon 2020 research and innovation programme under grant agreement No 850937, as well as from the Swiss SFOE-BFE project (SI/502310-01).

Open access funding provided by ETH-Bereich Forschungsanstalten.

Conflict of Interest

The authors declare no conflict of interest.

Data Availability Statement

The data that support the findings of this study are available from the corresponding author upon reasonable request.

Keywords

Cd-free buffers, Cu(In, Ga)Se₂, lifetime, sputter damage

Received: March 24, 2022

Revised: May 20, 2022

Published online: June 15, 2022

- [1] M. Nakamura, K. Yamaguchi, Y. Kimoto, Y. Yasaki, T. Kato, H. Sugimoto, *IEEE J. Photovoltaics* **2019**, 9, 1.

- [2] T. Feurer, P. Reinhard, E. Avancini, B. Bissig, J. Löckinger, P. Fuchs, R. Carron, T. P. Weiss, J. Perrenoud, S. Stutterheim, S. Buecheler, A. N. Tiwari, *Prog. Photovoltaics Res. Appl.* **2017**, 25, 645.
- [3] J. Chantana, Y. Kawano, T. Nishimura, Y. Kimoto, T. Kato, H. Sugimoto, T. Minemoto, *Prog. Photovoltaics Res. Appl.* **2019**, 28, 3210.
- [4] J. Löckinger, S. Nishiwaki, T. P. Weiss, B. Bissig, Y. E. Romanyuk, S. Buecheler, A. N. Tiwari, *Sol. Energy Mater. Sol. Cells* **2017**, 174, 379.
- [5] T. Minemoto, A. Okamoto, H. Takakura, *Thin Solid Films* **2011**, 519, 7568.
- [6] T. Minemoto, J. Julayhi, *Curr. Appl. Phys.* **2013**, 13, 103.
- [7] T. Nakada, T. Kumazawa, H. Yamaguchi, T. Kobayashi, *IEEE J. Photovoltaics* **2013**, 3, 461.
- [8] M. Sugiyama, H. Sakakura, S.-W. Chang, *Electrochim. Acta* **2014**, 131, 236.
- [9] E. Aydin, C. Altinkaya, Y. Smirnov, M. A. Yaqin, K. P. S. Zanon, A. Paliwal, Y. Firdaus, T. G. Allen, T. D. Anthopoulos, H. J. Bolink, M. Morales-Masis, S. De Wolf, *Matter* **2021**, 4, 3549.
- [10] H. Kanda, A. Uzum, A. K. Baranwal, T. A. N. Peiris, T. Umeyama, H. Imahori, H. Segawa, T. Miyasaka, S. Ito, *J. Phys. Chem. C* **2016**, 120, 28441.
- [11] B.-M. Meiners, S. Holinski, P. Schäfer, S. Hohage, D. Borchert, Technical Report, **2015**.
- [12] W. Witte, W. Hempel, S. Paetel, R. Menner, D. Hariskos, *ECS J. Solid State Sci. Technol.* **2021**, 10, 055006.
- [13] K. Ramanathan, J. Mann, S. Glynn, S. Christensen, J. Pankow, J. Li, J. Scharf, L. Mansfield, M. Contreras, R. Noufi, in *Conf. Record of the IEEE Photovoltaic Specialists Conf.*, IEEE **2012**, pp. 1677–1680.

- [14] D. Hariskos, S. Spiering, M. Powalla, *Thin Solid Films* **2005**, 480–481, 99.
- [15] R. Carron, S. Nishiwaki, T. Feurer, R. Hertwig, E. Avancini, J. Löckinger, S.-C. Yang, S. Buecheler, A. N. Tiwari, *Adv. Mater.* **2019**, 9, 1900408.
- [16] U. Rau, *Phys. Rev. B* **2007**, 76, 085303.
- [17] M. Burgelman, P. Nollet, S. Degraeve. Technical Report, ELIS, University of Gent, **2000**.
- [18] R. Hertwig, S. Nishiwaki, M. Ochoa, S.-C. Yang, T. Feurer, E. Gilshtein, A. N. Tiwari, R. Carron, *EPJ Photovoltaics* **2020**, 11, 12.
- [19] P. J. Cullen, V. Milosavljević, *Prog. Theor. Exp. Phys.* **2015**, 2015, 063J01.
- [20] F. Lebreton, S. N. Abolmasov, F. Silva, P. Roca I Cabarrocas, *Appl. Phys. Lett.* **2016**, 108, 051603.
- [21] J. Serhan, Z. Djebbour, A. Darga, D. Mencaraglia, N. Naghavi, G. Renou, D. Lincot, J. F. Guillemeoles, *Sol. Energy Mater. Sol. Cells* **2010**, 94, 1884.
- [22] I. Repins, S. Glynn, T. J. Silverman, R. Garris, K. Bowers, B. Stevens, L. Mansfield, *Prog. Photovoltaics Res. Appl.* **2019**, 27, 749.
- [23] W. J. Lee, D. H. Cho, J. M. Bae, M. E. Kim, J. Park, Y. D. Chung, *Nano Energy* **2020**, 74, 104855.
- [24] T. Lavrenko, T. Walter, B. Plesz, *Phys. Status Solidi C* **2017**, 14.
- [25] T. Welzel, R. Kleinhempel, T. Dunger, F. Richter, *Plasma Processes Polym.* **2009**, 6 S331.
- [26] T. Welzel, T. Dunger, B. Liebig, F. Richter, *Plasma Sources Science And Technology Determination of Energy Modulations of Negative Oxygen Ions During Pulsed Magnetron Sputtering of Magnesium Oxide*, IOP Publishing, **2011**.
- [27] T. Welzel, K. Ellmer, *J. Phys. D: Appl. Phys.* **2013**, 46, 315202.
- [28] R. Scheer, H.-W. Schock, *Chalcogenide Photovoltaics*, Wiley-VCH Verlag GmbH & Co. KGaA, Weinheim, Germany **2011**.
- [29] S. Schorr, *Crystallography in Materials Science*, De Gruyter **2021**.
- [30] T. L. Cottrell. Technical report, Butterworths **1958**.
- [31] Y.-R. Luo. Technical report, **2009**.
- [32] J. M. Woodall, G. D. Pettit, T. N. Jackson, C. Lanza, K. L. Kavanagh, J. W. Mayer, *Phys. Rev. Lett.* **1983**, 51, 1783.
- [33] I. M. Dharmadasa, J. D. Bunning, A. P. Samantilleke, T. Shen, *Sol. Energy Mater. Sol. Cells* **2005**, 86, 373.
- [34] I. M. Dharmadasa, *Semicond. Sci. Technol.* **2009**, 24, 55016.
- [35] I. Moeini, M. Ahmadvpour, N. E. Gorji, *Superlattices Microstruct.* **2018**, 117, 399.
- [36] R. Herberholz, M. Igalsen, H. W. Schock, *J. Appl. Phys.* **1998**, 83, 318.
- [37] M. Turcu, U. Rau, in *Springer Series in Materials Science*, Vol. 86, Springer Verlag **2006**, pp. 91–111.
- [38] T. Eisenbarth, T. Unold, R. Caballero, C. A. Kaufmann, H. W. Schock, *J. Appl. Phys.* **2010**, 107, 034509.
- [39] J. Pettersson, C. Platzer-Björkman, U. Zimmermann, M. Edoff, *Thin Solid Films* **2011**, 519, 7476.
- [40] J. Li, Y. Ma, G. Chen, J. Gong, X. Wang, Y. Kong, X. Ma, K. Wang, W. Li, C. Yang, X. Xiao, *Sol. RRL* **2019**, 3, 1800254.
- [41] Y. Zhang, Y. Zhang, X. Chen, S. Wang, Q. Gao, M. Wu, Z. Wang, J. Ao, Y. Sun, W. Liu, Q. Zhang, *Mater. Sci. Semicond. Process.* **2022**, 140, 106380.
- [42] R. Kotipalli, B. Vermang, J. Joel, R. Rajkumar, M. Edoff, D. Flandre, *AIP Adv.* **2015**, 5, 107101.
- [43] F. Larsson, J. Keller, J. Olsson, O. Donzel-Gargand, N. M. Martin, M. Edoff, T. Törndahl, *Sol. Energy Mater. Sol. Cells* **2020**, 215, 110647.
- [44] P. M. Jundt, D. Kuciauskas, J. R. Sites, *IEEE J. Photovoltaics* **2022**, 12, 501.
- [45] T. P. Weiss, B. Bissig, T. Feurer, R. Carron, S. Buecheler, A. N. Tiwari, *Sci. Rep.* **2019**, 9, 1.
- [46] M. Zutter, J. Virtuoso, P. Anacleto, L. Yasin, M. Alves, M. Madeira, O. Bondarchuk, S. Mitra, D. F. Signes, J. M. Garcia, F. Briones, R. Waechter, O. Kiowski, D. Hariskos, D. Colombara, S. Sadewasser, *Phys. Status Solidi RRL* **2019**, 13, 1900145.